Chapter 2

Survey of Creep Cavitation in fcc Metals

Rolf Sandström and Junjing He

Additional information is available at the end of the chapter

http://dx.doi.org/10.5772/66592

Abstract

Cavitation plays an important role in plants operating at high temperatures since the cavitation controls the creep failure of engineering alloys. In the past it has been difficult to predict the cavitation behaviour with the help of basic models, since critical models have been missing. Recently new models have been formulated for grain boundary sliding, cavity nucleation and cavity growth to fill this gap. These models are reviewed in this chapter. It is shown that the new models can quantitatively predict cavitation for austenitic stainless steels, where detailed experimental information is available.

Keywords: creep, cavitation, grain boundary sliding, austenitic stainless steels, copper

1. Introduction

At temperatures above 0.4 of the absolute melting temperature T_m, materials are exposed to a slow plastic deformation called creep. For steel 0.4 T_m is about 500°C. The slow deformation takes place also at constant stress. Many important technical units operate at such high temperatures. This applies, for example, to fossil fired power plants that produce most of the world's electric power. Another example is gas turbines in aircrafts where the maximum metal temperature exceeds 900°C.

Due to creep the total strain in the material gradually increases. At the same time the microstructure can also change. For example the strength of many materials used at high temperatures is based on the presence of fine particles that slow down the deformation. There is a thermodynamic driving force for coarsening of the particles, since this will reduce the total surface area of the particles and thereby the surface energy. The deformation of the material and changes in the microstructure will decrease the strength of the material and this is referred to as the formation of creep damage. When the creep damage has reached a certain level, failure takes place.

Polycrystalline materials consist of regions with a specific lattice orientation called grains and the boundaries between them grain boundaries. During the creep deformation, small voids called creep cavities are formed at the grain boundaries. The size for the cavities is of the order 1 μm. The creep cavities are continuously nucleated so their number increases with time. Each individual cavity also grows so their radii increase. The driving force is the same as for coarsening of particles, that is, a reduction of the surface energy. In this way, there is a gradually increasing fraction of the grain boundaries that is cavitated. When the area fraction of cavities has reached a critical value, the cavities join and eventually form cracks that make the material fail.

The fact that creep rupture is mainly controlled by the development of grain boundary cavities has created a large technical interest in cavitation. This interest increased even more in the 1980s, when it was recognised that the appearance of the cavitation could be used to estimate the residual life time of fossil fired power plants. The service time of many power plants were approaching the design life and operators were asking whether it would be safe to continue running the plants. Neubauer found that by observation of the cavitation with the help of the replica technique, the residual lifetime could be estimated [1, 2]. The cavitation was subdivided into four classes (and one for undamaged material): individual cavities to a small extent, individual cavities to a large extent, stringers of cavities and finally microcracks. Replicas were taken at welds, pipe bends and other critical positions. The basic idea was that if damage of one class was detected, the damage did at most correspond to the next class at the next inspection. The method was very successful when it was applied to low alloy steels such as 0.5Cr0.5Mo0.25V and 2.25Cr1Mo, which represented the body of materials of the plants at the time. Unfortunately the method is less applicable to today's materials such as 9 and 12Cr steels, because cavitation appears only at a late stage of life and does not provide the necessary early warning.

The successful technical use of observations of cavitation stimulated a lot of scientific work. This was dominated by empirical approaches to describe the development of the creep damage. The first and perhaps most well-known approach was set up by Kachanow and Rabotnov [3–5]. They simply assumed that the cavities represented voids that reduced the loading capacity. The most interesting feature of the method is that it is consistent with behaviour of creep strain during the tertiary creep, that is, the final stage before rupture [6, 7]. This dependence is nowadays referred to as the omega method [8].

We will now concentrate on basic models for cavitation. Traditionally cavity nucleation has been modelled either as a process of rupturing atomic bonds or of atomic vacancy condensation. For the former approach the estimated threshold stress is orders of magnitude higher than the applied stress, which makes it physically unrealistic because high stresses will be reduced quickly in a creeping material [9]. The condensation of vacancies can be treated with the help of the classical nucleation theory [10]. It is shown that cavity nucleation would be a very rare event at low stresses but becomes frequent above a certain threshold stress [11]. High stress concentration can be formed at grain boundary ledges, grain boundary triple points and particles. Cavity nucleation at particles can be a result of decohesion of particles from the matrix. In practically all models that have been presented, a high stress concentration is needed.

http://dx.doi.org/10.5772/66592

A threshold stress and an incubation time are essential to form a cavity [10, 12]. Contrary to these suggestions nucleation frequently takes place at low stresses and is controlled by strain rather than stress. In agreement with statements in the literature it can be concluded that theories of cavity nucleation have not been fully successful in earlier work [13, 14]. In both these papers excellent reviews are given.

For modelling cavity growth the situation was different but not entirely unproblematic. A diffusion controlled cavity growth was formulated by Hull and Rimmer [15]. The model was later improved in particular by Beere and Speight [16]. It was soon realised that the model gave much larger growth rates than observed experimentally in many cases. Dyson proposed that the cavities should not be able to grow faster than the creep deformation of the surrounding material [17]. This is referred to as constrained cavity growth. Rice developed an explicit model for constrained growth [18]. The idea of constrained growth is now fully accepted. However, the model still tends to overestimate the growth rates. It is now believed to be due to the assumptions in Rice's derivation. This will be analysed in the present paper.

It is evident from the summary above that the modelling of formation and growth of cavities has met considerable difficulties in the past. In recent years important new developments have taken place. With the help of these developments fundamental quantitative modelling of both nucleation and growth of creep cavities has now been possible to set up. In addition some of the difficulties that have been encountered in the past can be understood. It is the purpose of this paper to review these new developments.

2. Grain boundary sliding

Grain boundary sliding (GBS) occurs when neighbouring grains move with respect to each other in shear. The mechanism is illustrated in **Figure 1**. During the creep deformation the two grains have moved 0.8 μm with respect to each other. To observe GBS, the specimen surface has to be scratched, for example, with a knife. When the scratches cross a sliding grain boundary, the two parts of the scratches on the different sides of the grain boundary are displaced. This displacement is a direct measure of GBS.

It is generally accepted that a prerequisite for cavity nucleation is grain boundary sliding. Experiments on copper bicrystals have shown that artificially introduced GBS can dramatically increase the amount of cavitation. Chen and Machlin [20] and Intrater and Machlin [21] exposed bicrystals of copper to either tensile loading or to a combination of tensile loading and shear. The latter alternative gave much larger number of cavities. It is natural that GBS gives rice to cavitation, since any obstacle at the grain boundary such as a particle will give rise to large stress concentrations. In low alloy steels cavities have frequently been observed around manganese sulphides [22]. Since the interface between the sulphides and the matrix is weak, voids are easily formed there. Some papers also suggest that cavities can be formed at carbides, see, for example, Ref. [23].

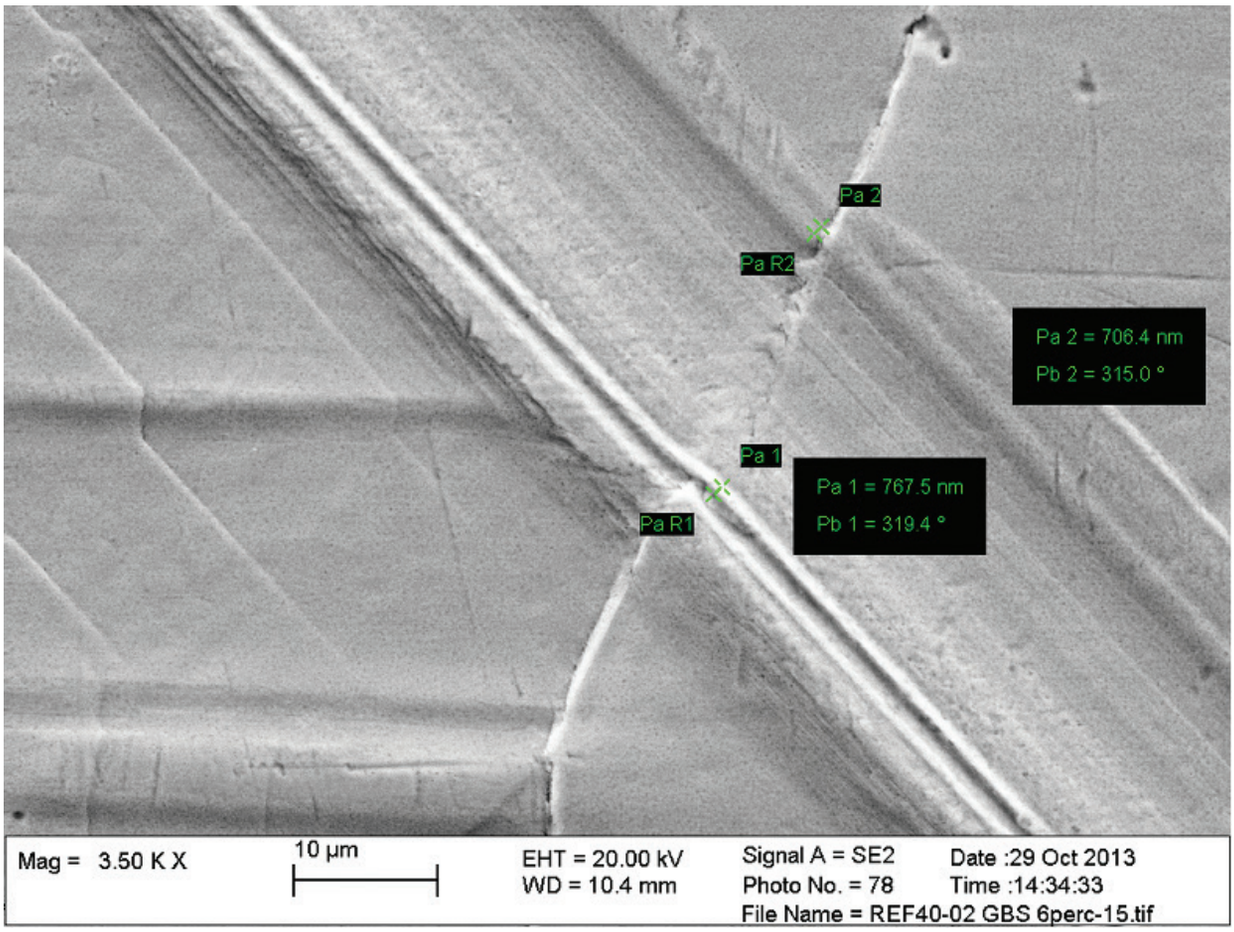

Figure 1. Illustration of grain boundary sliding (GBS) for a copper specimen that has been exposed to 3.3% creep strain during 307 h at 125°C [19]. The grain boundary lies in the southwest-northeast direction. It is crossed by a major scratch, which makes it possible to measure GBS. The grain to the left has moved downwards by 0.8 µm relative to the grain at the right and that is the amount of GBS.

The most convincing argument concerning the central role of GBS in cavity nucleation comes from the creep strain dependence of both GBS and cavity nucleation. It has been observed many times that the displacement u_{GBS} due to GBS is approximately proportional to the creep strain ε, see, for example, Ref. [24]. The first ones to observe this relation were McLean and Farmer [25].

$$u_{GBS} = C_s(\varepsilon)\varepsilon. \tag{1}$$

$C_s(\varepsilon)$ is a constant that is dependent on the creep strain ε. At the same time the nucleation rate of cavities $\frac{dn}{dt}$ is also proportional to the creep strain rate $\dot{\varepsilon}$.

$$\frac{dn}{dt} = B\dot{\varepsilon}. \tag{2}$$

B is constant. This means that the number of cavities is proportional to the creep strain in the same way as the GBS displacement in Eq. (1). Eq. (2) was first observed by Needham and

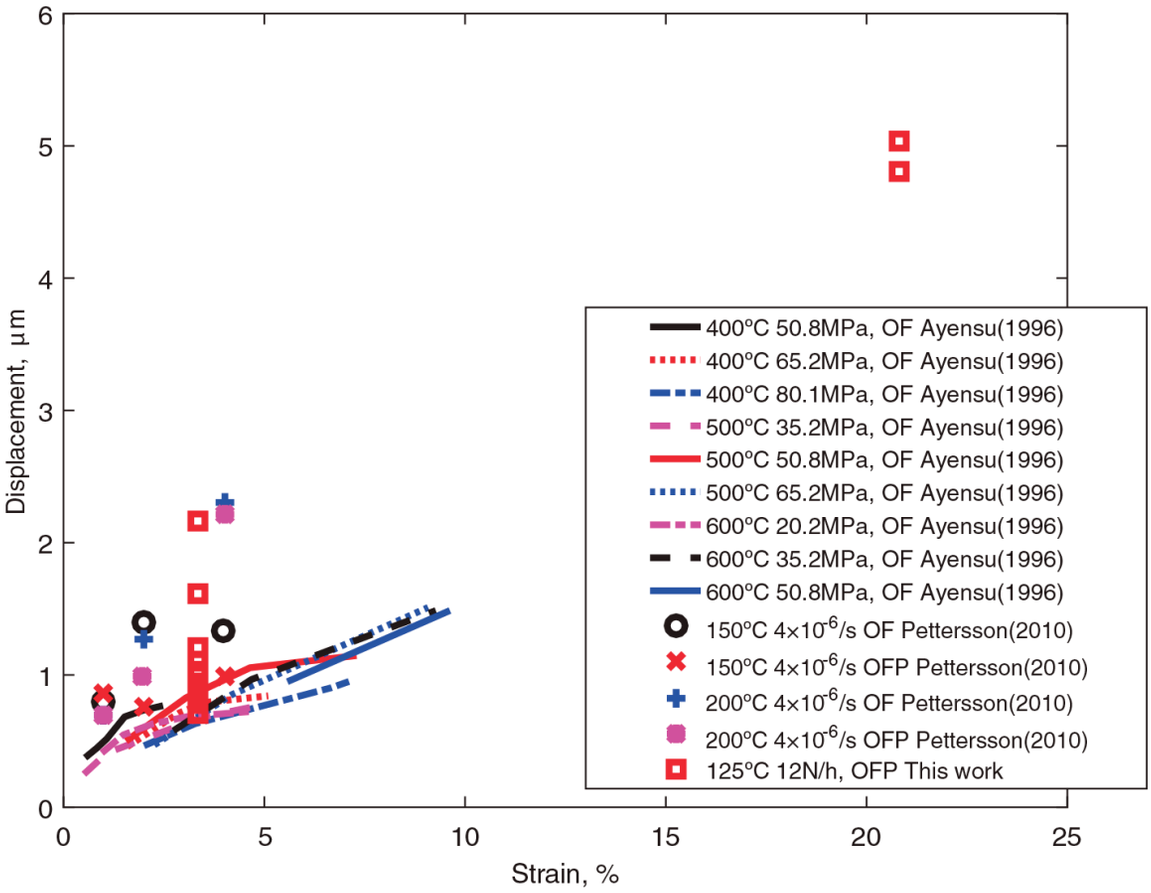

Figure 2. Observed displacements at grain boundaries in copper as a function of strain [19]. Data from Refs. [29, 30] are also shown.

coworkers [26, 27]. For a review, see Ref. [28]. Eqs. (1) and (2) will be derived below. Eq. (2) would be very difficult to explain unless it assumed that the nucleation is controlled by GBS.

Experiments that give the strain dependence of u_{GBS} are illustrated in **Figure 2**.

The displacement u_{GBS} increases as of function of strain in agreement with Eq. (1). C_s is the slope of the curves. Three types of tests are represented in the figure: tests at constant stress, at constant stress rate and at constant strain rate. In spite of the fact that a range of temperatures, strain rates and test methods is covered, the C_s values do not vary very much.

To investigate the influence of GBS on the total strain, Crossman and Ashby [31] developed a finite element model (FEM) for shear stresses. If a free grain boundary is considered, they found that the sliding rates are very high for typical creep stresses and that the grain boundaries could be considered as flaws in the material with respect to GBS. Later Ghahremani [32] transferred the model to tensile stresses, which are typically used in creep testing. In both Refs. [31, 32] a Norton equation for the creep strain rate was considered

$$\dot{\varepsilon} = \dot{\varepsilon}_0 \left(\frac{\sigma}{\sigma_0}\right)^n. \tag{3}$$

σ is the applied stress and n is the creep exponent. $\dot{\varepsilon}_0$ and σ_0 are constants. The percentage creep rate due to grain boundary sliding ϕ was determined

$$\phi = \frac{\dot{u}_{\mathrm{GBS}}}{\dot{u}_{\mathrm{all}}}. \tag{4}$$

$\dot{u}_{\mathrm{all}}$ is the total displacement rate. ϕ was found to take values from 0.15 ($n = 1$) to 0.33 ($n = \infty$) in Ref. [32]. $\dot{u}_{\mathrm{all}}$ can be expressed in terms of the creep rate $\dot{\varepsilon}$

$$\dot{u}_{\mathrm{all}} = \frac{3\, d_{\mathrm{lin}}\, \dot{\varepsilon}}{2\xi}, \tag{5}$$

where d_{lin} is the linear intercept grain size and $\xi = 1.36$ is a pure geometrical factor that explains how the hexagonal grains studied in Refs. [31, 32] should be related to the measured grain size. The factor 3/2 depends on the definition of $\dot{u}_{\mathrm{all}}$. By combining Eqs. (1), (4) and (5) we find the values of the GBS parameter C_s in Eq. (1)

$$C_s = \dot{u}_{\mathrm{GBS}} \Big/ \dot{\varepsilon} = \frac{3\phi}{2\xi} d_{\mathrm{lin}}. \tag{6}$$

Eq. (6) is referred to the *shear sliding model*. Eq. (6) is compared with experimental results for copper in **Figure 3**. The C_s values according to Eq. (6) for the individual tests in **Figure 2** have

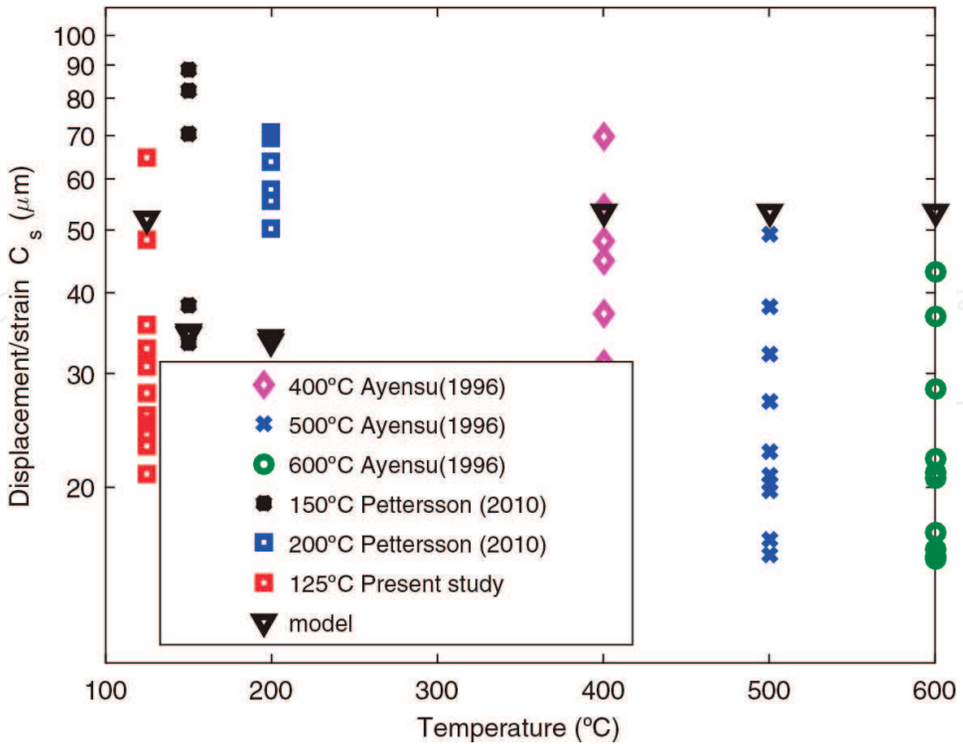

Figure 3. Comparison of modelled Eq. (6) and observed displacements at grain boundaries in copper divided by the creep strain, cf. Eq. (1) [19]. Data from [29, 30] are also shown.

been evaluated in [19]. The model values are about $C_s \approx 50$ μm. These values are slightly high for the creep tests [30], but in range for slow strain tests [29] and constant stress rate tests [19].

For materials with particles in the grain boundaries Riedel has derived a model corresponding to Eq. (1) [33]. The sliding boundary was represented by a shear crack surrounded by creep deforming grains. The model is referred to as the *shear crack model*. Although the author was not very happy with the model, it turns out that it does not give very different results for austenitic stainless steels in comparison with the shear sliding model.

The two models (shear sliding and shear crack models) are compared with the experimental GBS displacements for different austenitic stainless steels [34–38] in **Figure 4**. The shear crack model is compared with the average of all the experimental data, Ave. 1. The shear sliding model does not work very well for large grain sizes so data for such grain sizes [38] are not included in the comparison, Ave. 2. It can be seen from **Figure 4** that C_s values of the correct order are predicted.

From **Figures 3** and **4** it is evident that the shear sliding and shear crack models can describe the experimental data for fcc metals with reasonable precision.

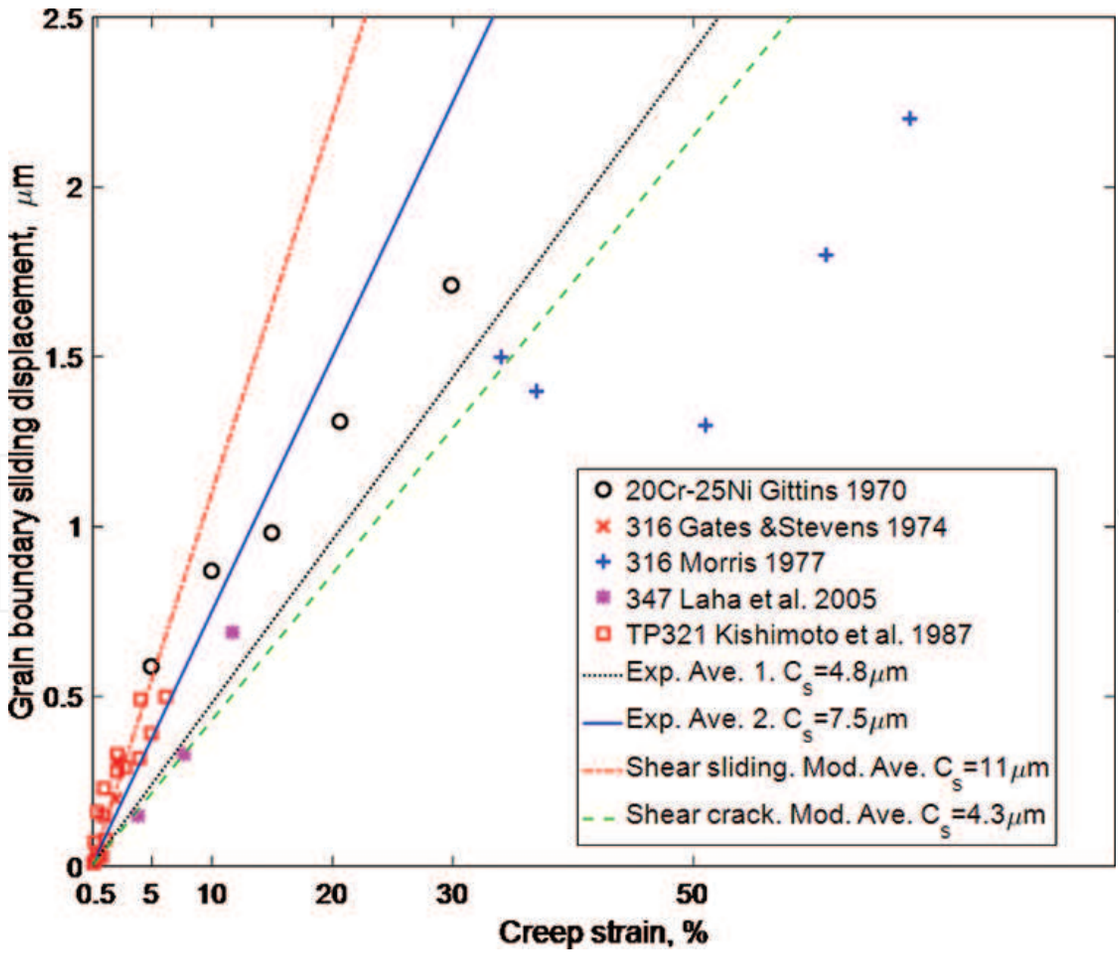

Figure 4. Modelling and experimental GBS displacement as a function of creep strain for different types of austenitic stainless steels, from Ref. [24]. Experimental data Ref. [34–38].

3. Cavity nucleation

3.1. Thermodynamic considerations

The mechanisms for cavitation nucleation have been a puzzle for a long time as explained in the introduction. However part of the explanation came from studies on copper. Pure copper can show extensive cavitation during creep [39], but the number of particles present is so low that they cannot explain the large number of cavities. Lim suggested that it was the substructure of the dislocations that could nucleate the cavities [40]. He also presented a model that can be used to demonstrate whether a nucleation mechanism is thermodynamically feasible or not. He assumed that pile ups of grain boundary dislocations generate the necessary high stresses for the nucleation. Since these high stresses are stationary as a result of the creep process, it avoids the problem of fast stress relaxation in many models. Lim's model is fairly complex and details in the model will not be given here. When a cavity is formed the free energy ΔG is changed in a number of ways that are represented by the terms in the following equation [19]

$$\Delta G = -r^3 F_v \sigma_{appl} + r^2 F_s \gamma_s - r^2 F_{GB} \gamma_{GB} - (\Delta G_1 + \Delta G_2 + \Delta G_3). \quad (7)$$

γ_s and γ_{GB} are the surface and grain boundary energies per unit area. $F_v = 2\pi/3\ (2–3\cos\alpha + \cos^3\alpha)$, $F_s = 4\pi(1-\cos\alpha)$, $F_b = \pi\sin^2\alpha$ and $F_v' = 1.5\ F_v$, where α is half the tip angle of the cavity. The first term in Eq. (7) is the work done by the applied stress. The second and third terms represent the modification in the surface and grain boundary energies. The fourth term is the decrease in the strain energy. ΔG_1 is the change in the line energy of the grain boundary dislocations (GBD). ΔG_2 is the interaction energy between the remaining and the consumed GBD. The strain energy ΔG_3 is the reduction of the strain energy of GBDs outside the cavity. Full details can be found in [19, 40].

Lim's model has been applied to copper and austenitic stainless. As long as energy is gained when a cavity is formed, that is, ΔG in Eq. (7) is negative, cavitation is possible. From Eq. (7) ΔG is reduced when the applied stress σ_{appl} is raised, that is, cavitation becomes more likely which is natural. On the other hand when σ_{appl} is reduced cavitation is more difficult. There is minimum stress where cavitation is no longer possible because ΔG becomes positive. This minimum stress is plotted as a function of temperature for copper in **Figure 5**.

These minimum stresses are compared with design stresses during creep in copper. It is clear that the stresses required for nucleation are well below the stresses that typically appear in the material. This demonstrates that nucleation based on the substructure is a viable process.

From a technical point of view it is well established that the creep ductility of oxygen free pure copper Cu-OF can be very much lower than for phosphorus alloyed copper Cu-OFP. As a consequence the latter material should be used in creep exposed components [28, 41]. It is evident from **Figure 5** that much lower stresses are needed in Cu-OF than in Cu-OFP, which makes the cavitation in the former material much more abundant. This is believed to be the main reason for the low creep ductility of Cu-OF.

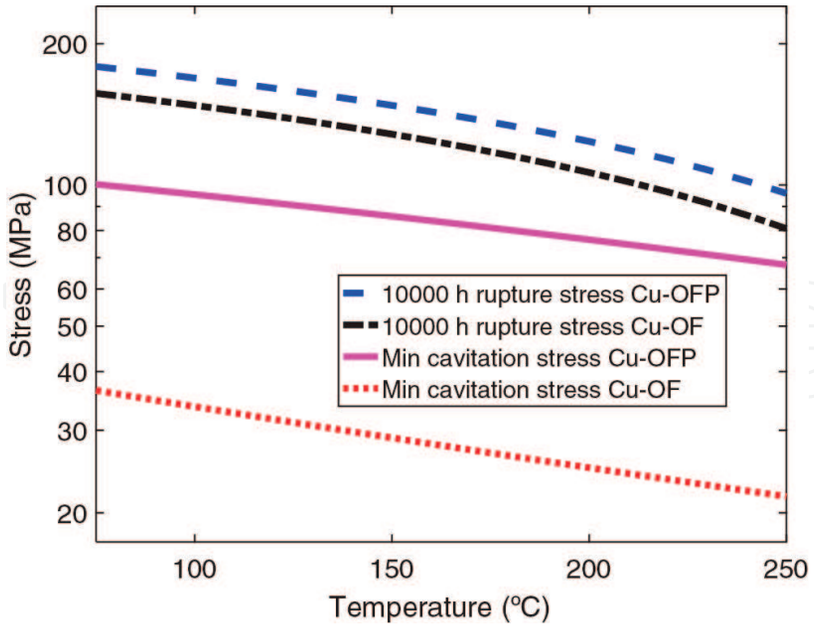

Figure 5. Minimum stress to form cavities at cell boundaries versus temperature for oxygen free pure Cu-OF and phosphorus alloyed copper Cu-OFP. For comparison the stress that gives creep rupture after one year (10,000 h) is included. After Ref. [19].

It has also been verified that the minimum nucleation stresses are below typical design stresses for the common stainless steels 304H (18Cr10Ni), 316 (17Cr12Ni2Mo), 321 (18Cr12NiTi) and 347 (18Cr12NiNb). For example this is illustrated for 347 (18Cr12NiNb) in **Figure 6**. The design stresses are 10,000 h rupture data. The minimum cavitation stress lies in the interval 35–50 MPa in the interval from 500°C to 750°C. The minimum cavitation stresses are again below the design stresses. The temperature dependence of Lim's model is probably not fully correct. In general it is thought that the amount of cavitation will increase with temperature. However the temperature dependence of the minimum cavitation stress is weaker than that of the design stress, which suggests the opposite behaviour.

3.2. Strain dependence

Experimentally it has been found many times that the number of cavities is proportional to the creep strain, cf. Eq. (2). To explain this strain dependence, Sandstrom and Wu introduced the *double ledge model* [43]. They considered a sliding grain boundary with dislocation substructures on both sides of the boundary that moved along with the grains. The substructures consist of subgrains that contain fairly few dislocations in their interior but with well-developed subgrain walls. The positions where the subgrain walls meet at the grain boundary are referred to as subgrain corners. Nucleation was assumed to take place when a subboundary on one side of the boundary hits a subgrain corner on the other side. The nucleation rate can be expressed as

$$\frac{dn}{dt} = \frac{\dot{u}_{GBS}}{d_{sub}} \frac{1}{d_{sub}^2}, \tag{8}$$

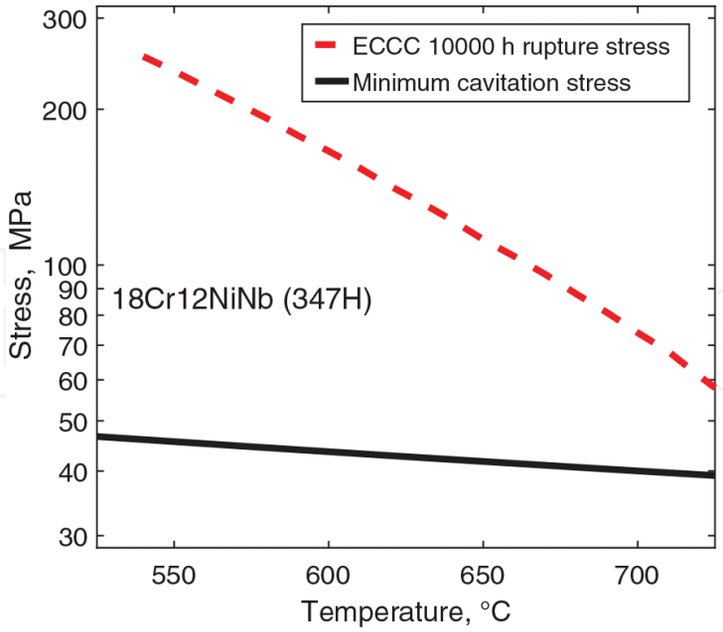

Figure 6. Minimum cavitation stress versus temperature for TP347H austenitic stainless steel. 10,000 h rupture data from ECCC [42] for TP347 are shown for comparison.

where d_{sub} is the subgrain diameter. The last factor takes into account that one nucleus can be formed in each subgrain on the boundary. The subgrain size is directly related to the applied stress [19]

$$d_{sub} = K_{sub} GB/\sigma_{appl}. \tag{9}$$

The constant K_{sub} is about 20 for austenitic stainless steels and about 11 for copper. The same model can be applied to particles in the grain boundary that are known to contribute to the nucleation. In the model the subgrain corners are replaced by the particles in the grain boundaries with an interparticle distance of λ. Taking both subgrain corners and particles into account, the resulting expression for the nucleation rate is [44]

$$\frac{dn}{dt} = \frac{0.9\, C_s}{d_{sub}}\left(\frac{1}{d_{sub}^2} + \frac{1}{\lambda^2}\right)\dot{\varepsilon} = B\dot{\varepsilon}. \tag{10}$$

In Eq. (10), Eq. (1) has been used. The factor 0.9 in Eq. (10) takes into account the averaging of different orientations [44].

The model in Eq. (10) is compared with experimental data for austenitic stainless steels in **Figure 7**. For three of the experimental data sets TP347 at 550°C and 650°C and TP304 at 727°C, the model gives quite an acceptable description. For TP304XX at 750°C the deviation between model and experiment is larger.

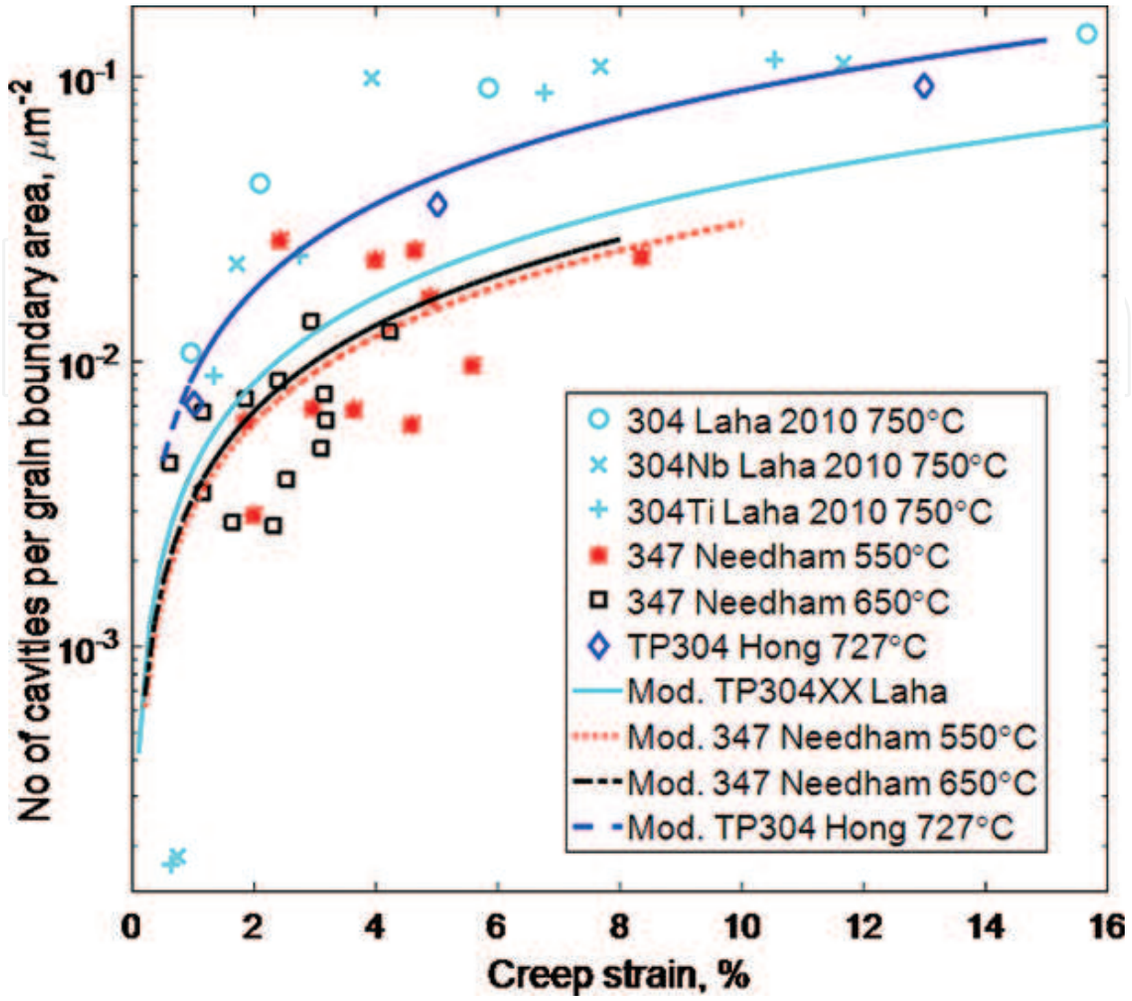

Figure 7. Modelling and experimental number of cavities per unit grain boundary area as a function of creep strain [44]. Experimental data from Hong and Nam [45] for TP304 steel, Laha et al. [46] for three different types of austenitic stainless steels and Needham and Gladman [27] for TP347 steel.

3.3. Particle size

It has been proposed that a critical particle radius exists for nucleation [45, 46]. The radius must exceed a minimum value in order for nucleation to take place. Harris developed a model that related the critical particle size to the GBS velocity [47, 48]. His basic assumption was that particles are not able to stop GBS if the diffusion is fast enough. According to Harris this critical particle radius also represented the minimum radius that could nucleate cavities. Harris gave the following relation between the GBS velocity $\dot{u}_{GBS}$ and the critical particle radius r_c

$$\dot{u}_{GBS} = \frac{\delta D_{GB}}{r_c^2 \ln\frac{\lambda}{2r_c}}\left(\exp\frac{2\gamma_s \Omega}{k_B T r_c} - 1\right), \tag{11}$$

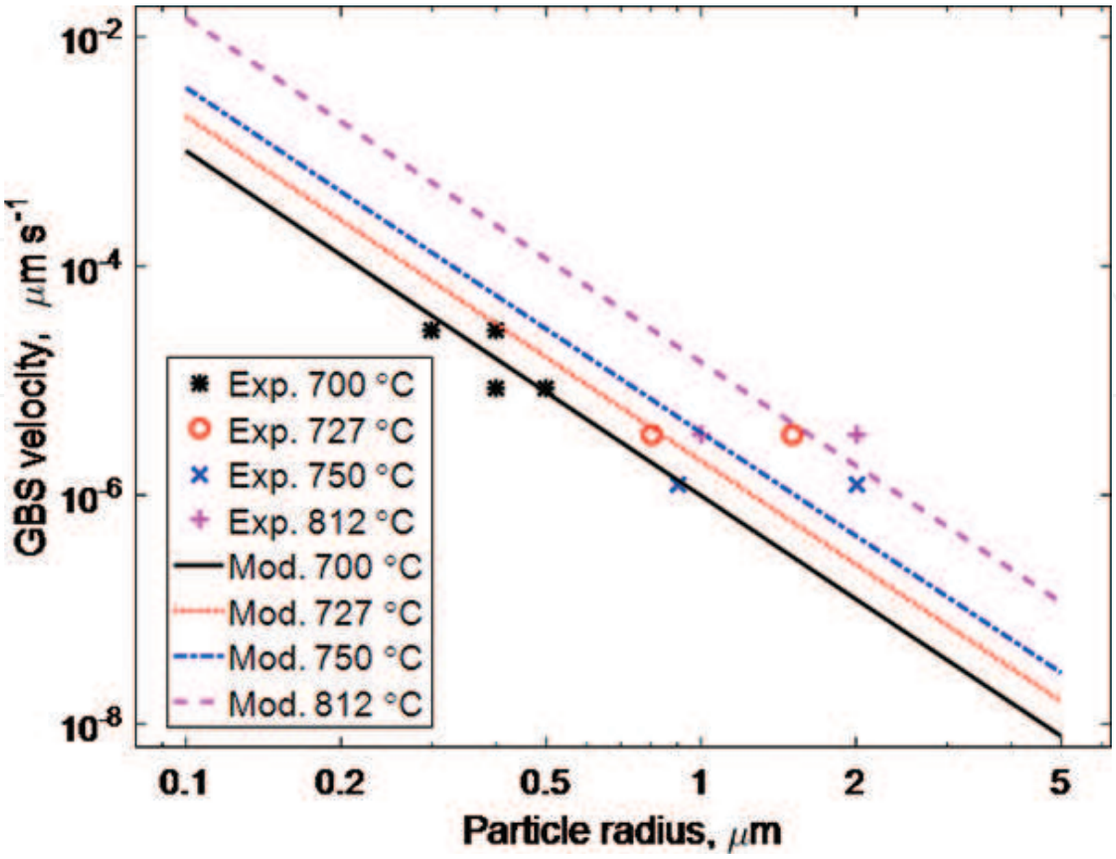

Figure 8. Comparison of experimental and modelling GBS velocity as a function of particle radius [24]. Experimental data for 304, 321 and 347 austenitic stainless steels from Refs. [45, 46, 49, 50]. Modelling results from Eq. (11).

where λ is the interpaticle spacing, γ_s the surface energy, δ the grain boundary width, D_{GB} the grain boundary self-diffusion coefficient, Ω the atomic volume, k_B Boltzmann's constant and T the absolute temperature. The application of Eq. (11) is illustrated in **Figure 8** for different types of austenitic stainless steels [24].

In **Figure 8** the particle parameters are taken from the experimental references. The minimum particles that nucleated cavities in the experiments are chosen for the critical particle radius. The experimental data clearly support Harris' model.

From the particle size distributions [24] the number of nucleated cavities can be estimated if the critical particle size is known. The computed number of nuclei is compared with the observed ones for austenitic stainless steels in **Figure 9.**

4. Cavity growth

4.1. Unconstrained cavity growth model

After the cavities have been nucleated, they start to grow if they exceed a critical size. The main mechanism for the growth is diffusion. Vacancies are transported away from the surfaces of the cavities. The grain boundaries are good sinks for the vacancies. The first model for

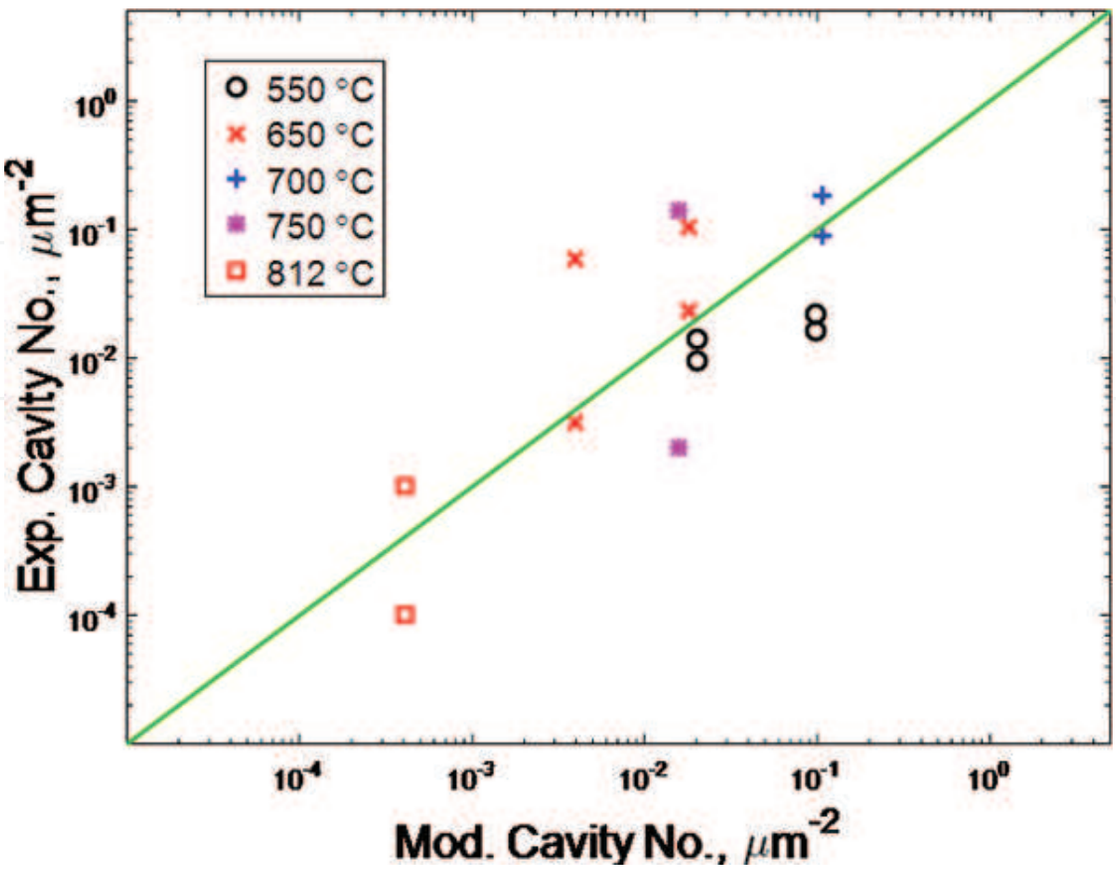

Figure 9. Comparison of experimental number of cavities and modelling number of particles that initiate cavities [24]. Experimental data for austenitic stainless steels from Refs. [27, 45, 46, 49, 50].

diffusion controlled growth was presented by Hull and Rimmer [15]. A much more elegant formulation was later given by Beere and Speight [16] and this is the model that has been used since. Their growth equation can be expressed as

$$\frac{dR}{dt} = 2 D_0 K_f(\sigma_{appl} - \sigma_0) \frac{1}{R^2}, \tag{12}$$

where R the cavity radius in the grain boundary plane, dR/dt its growth rate, σ_0 the sintering stress $2\gamma_s \sin(\alpha)/R$, where γ_s is the surface energy of the cavity per unit area and α the cavity tip angle. D_0 is a grain boundary diffusion parameter, $D_0 = \delta D_{GB}\Omega/k_B T$, where δ is the grain boundary width, D_{GB} the grain boundary self-diffusion coefficient, Ω the atomic volume, k_B Boltzmann's constant and T the absolute temperature. The factor K_f was introduced in [16]. It is a function of the cavitated grain boundary area fraction $f_a = (2R/L)^2$

$$K_f = -1/\left[2 \log f_a + (1 - f_a)(3 - f_a)\right]. \tag{13}$$

From the number of cavities per unit grain boundary area n_{cav}, the cavity spacing L can be determined

$$L = 1/\sqrt{n_{cav}}\,. \tag{14}$$

n_{cav} can be found from the nucleation model, Eq. (10). Plastic deformation can also contribute to the growth rate. Danavan and Solomon have given an expression for that [51]

$$\frac{dR}{dt} = \frac{\sin^2(\alpha)}{\alpha - \sin(\alpha)\cos(\alpha)}\frac{R}{3}\dot{\varepsilon}\,. \tag{15}$$

4.2. Constrained cavity growth

When diffusion controlled growth models were compared with experimental data, it was evident that the models often strongly exaggerated the growth rate. Dyson found that the predicted growth rate of the cavities many times exceeded the deformation rate of the surrounding material which he considered as unphysical [17]. He suggested that the cavity growth rate should not be larger than the creep rate of the material. This was referred to as constrained growth. Based on this assumption, Rice developed a quantitative model [18]. The result is that in the growth equation, the applied stress is replaced by a reduced stress

$$\frac{dR}{dt} = 2D_0 K_f(\sigma_{red} - \sigma_0)\frac{1}{R^2}\,. \tag{16}$$

The reduced stress is given by

$$\sigma_{red} = \sigma_0 + \frac{1}{\frac{1}{\sigma_{appl}} + \frac{32 D_0 K_f}{L^2 d\beta\,\dot{\varepsilon}(\sigma_{appl})}}\,, \tag{17}$$

where β is a material constant (β = 1.8 for homogeneous materials) and d the grain diameter. With this approach a growth model that fulfils Dyson's criterion has been achieved.

Rice based his analysis on a linear viscoplastic model of an opening crack. He and Sandstrom reanalyzed the model and avoided the assumption of linearity [52]. A grain structure with a pillar of height h and width corresponding to the grain size d was set up. In this pillar the creep deformation in the axial (z) direction is given by

$$\frac{dz}{dt} = 4\pi D_0 K_f(\sigma_{red} - \sigma_0)\, n_{cav} + h\,\dot{\varepsilon}(\sigma_{red}) = h\,\dot{\varepsilon}(\sigma_{appl}). \tag{18}$$

$\dot{\varepsilon}(\sigma_{red})$ and $\dot{\varepsilon}(\sigma_{appl})$ are the creep rates at the reduced and applied stress, respectively. The first term in the middle part of Eq. (17) is the volume growth rate of a cavity multiplied by the number of cavities per unit grain boundary area. The creep displacement of the pillar at the reduced stress is the second term. The final term on the right hand is the displacement in the surrounding material. A finite element analysis was performed to determine the size of

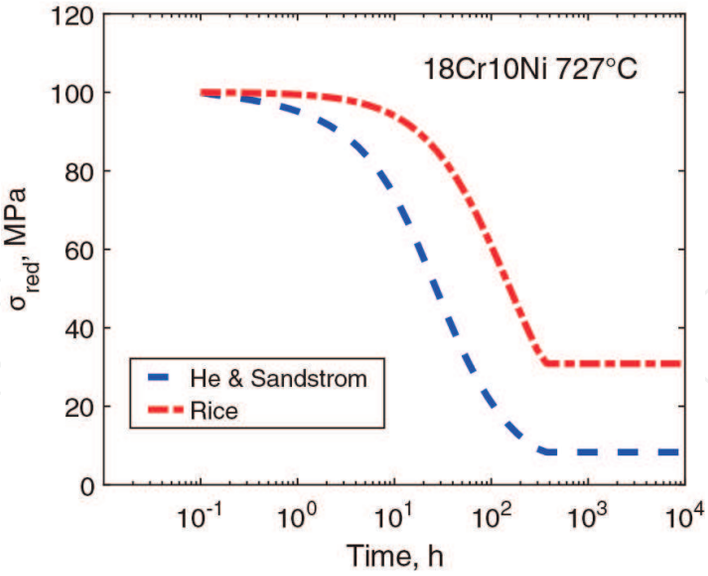

Figure 10. Reduced stress according to Eq. (19) versus time [52]. The result is compared with the model of Rice in Eq. (17) [18]. Cavity growth for 18Cr10Ni at 727°C and 100 MPa [45].

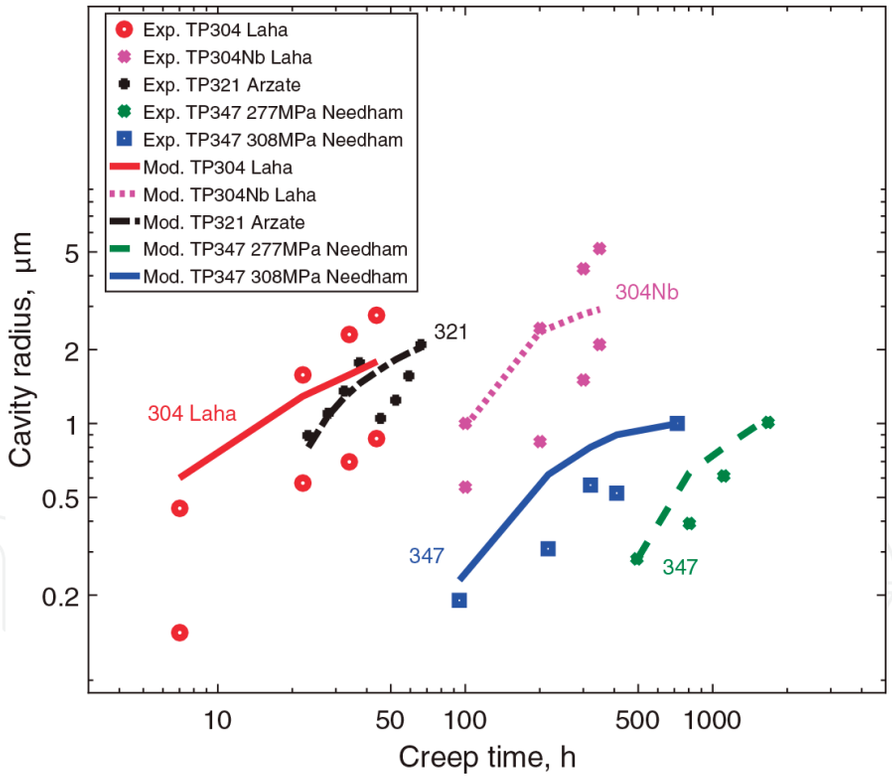

Figure 11. Cavity radius as a function of creep time for 18Cr10Ni without or with Nb (347) or Ti (321) austenitic stainless steels. Model according to Eq. (19) and experimental data from Refs. [27, 46, 49]. The creep tests were performed at temperatures in the interval of 650–812°C.

the height h. It was found that $h \approx 2R$ in the investigated cases [52]. If this value for h is used and n_{cav} is replaced by $1/L^2$ according to Eq. (14), the following equation is obtained

$$2\pi D_0 K_f(\sigma_{red} - \sigma_0) \Big| L^2 R + \dot{\varepsilon}(\sigma_{red}) = \dot{\varepsilon}(\sigma_{appl}). \quad (19)$$

In general Eq. (19) has to be solved by iteration to find the new value of σ_{red}. This new value for σ_{red} is lower than that given by Eq. (17). This is illustrated in **Figure 10**: Both the absolute and relative difference increase with time.

The new constrained growth model is compared to experimental data for austenitic stainless steels in [52]. Some examples are given here in **Figure 11**. Growth data for 18Cr10Ni steel with and without Nb or Ti are shown. It can be seen that the growth data can be described with fair accuracy. The lower growth rate according Eq. (19) is important in this respect.

5. Brittle creep rupture

Creep rupture is technically very important, because it determines the life of many plants operating at high temperatures. Two main mechanisms are distinguished: ductile rupture and brittle rupture. Ductile rupture is controlled by the exhaustion of the deformation capacity of the material. In this case the usual rupture criterion is that the creep strain reaches a critical value. The deformation takes place by dislocation mechanisms. The faster the dislocations move, the faster rupture occurs. Since ductile rupture does not involve cavitation, it is not reviewed here, but full details can be found elsewhere [53].

Rupture curves for dislocation creep are illustrated in **Figure 12** for the austenitic stainless steel 18Cr12NiTi (321H) at temperatures between 600°C and 775°C. The experimental creep rupture data cover times up to 100,000 h (11 years). The general overall behaviour is well described by the model predictions.

The second process brittle rupture is due to grain boundary decohesion. By far the most important mechanism in this respect is the formation and growth of cavities. It is well established that when the cavitated grain boundary area reaches a certain fraction of about 0.25, brittle rupture takes place [54]. The cavitated area fraction A_{cav} can be computed from Ref. [43]

$$A_{cav} = \int_{t_i}^{t} \frac{dn}{dt'}(t')\pi R^2(t, t')dt'. \quad (20)$$

A continuous nucleation of cavities takes place. The number of cavities is directly proportional to the creep strain, Eq. (10). Once a cavity has nucleated it starts to grow after an incubation time t_i that is a small fraction of the rupture time [52]. The growth is described with Eq. (16) with the reduced stress given by Eq. (19). When A_{cav} has reached 0.25, rupture is assumed to take place.

The model predictions for brittle rupture for 18Cr12NiTi (321H) are shown in **Figure 13**. The predictions are compared to the same experimental data as in **Figure 12**. Again the overall

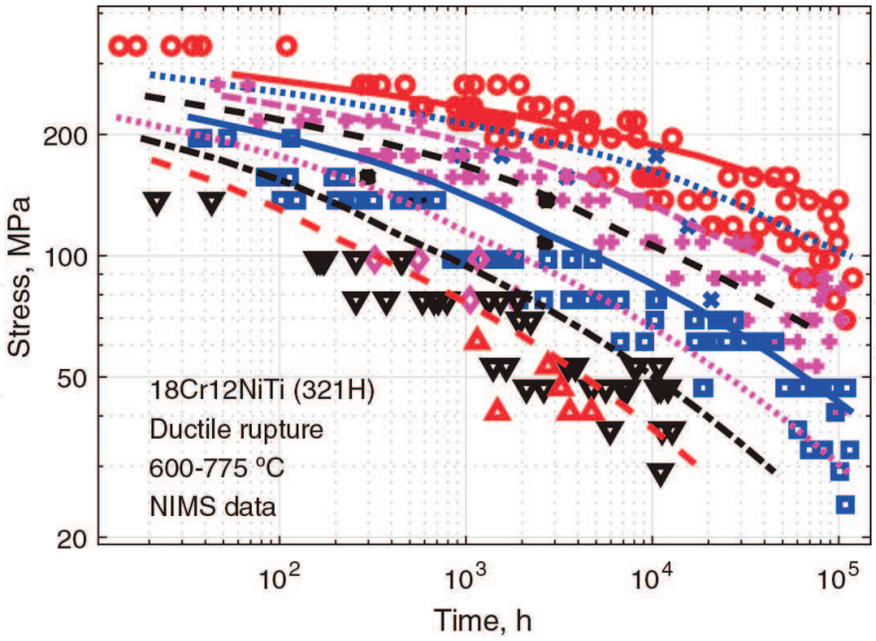

Figure 12. Comparison of dislocation creep model rupture curves (ductile rupture) Refs. [53, 54] with experiments [55] for 18Cr12NiTi (321H). Model prediction and experiments at temperatures between 600°C and 775°C with 25°C interval.

time dependence of the rupture strength at different temperatures is well represented. In fact the differences between the model predictions for ductile rupture in **Figure 12** and brittle rupture **Figure 13** are not very large.

Ductile rupture is assumed to be controlling if the strain exhaustion occurs before $A_{cav} = 0.25$ has been reached. On the other hand if the cavitation criterion is reached first, brittle rupture takes place. The results for ductile and brittle rupture are combined in **Figure 14**. For a given

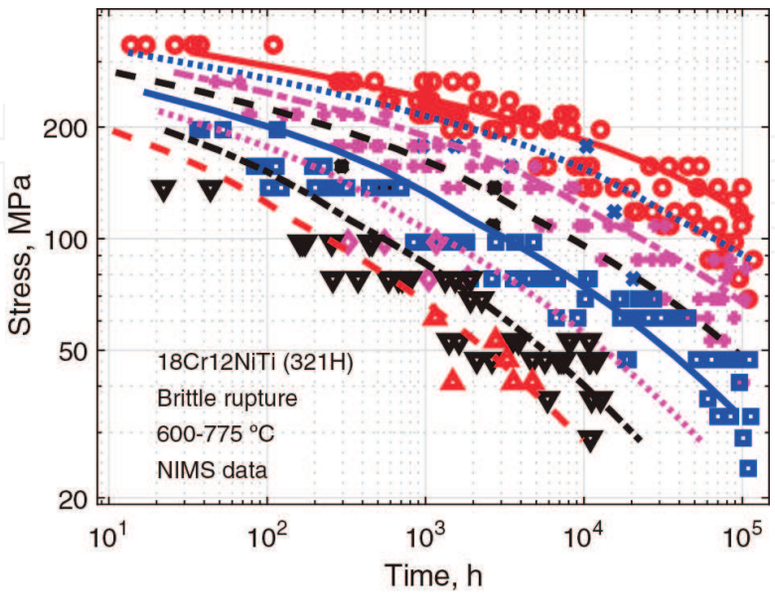

Figure 13. Comparison of model rupture curves based on cavitation (Eq. (20), brittle rupture) [54] with experiments [55] for 18Cr12NiTi (321H). Model prediction and experiments at temperatures between 600°C and 775°C with 25°C interval.

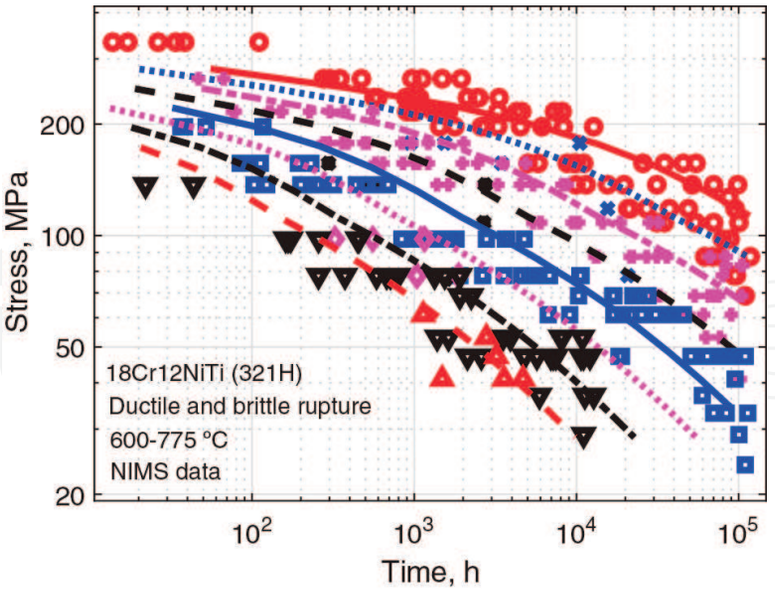

Figure 14. Comparison of model rupture curves based on both dislocation creep (ductile rupture) and cavitation (brittle rupture) with experiments [55] for 18Cr12NiTi (321H). Model predictions and experiments at temperatures between 600°C and 775°C with 25°C interval.

temperature and stress the value from **Figure 12** is chosen if the (ductile) rupture time is shorter than the (brittle) rupture time in **Figure 13** and vice versa.

When brittle rupture is taken into account when modelling the creep rupture curves, there is an improvement in particular at high temperatures and low stresses.

6. Discussion

With the development of the *shear sliding* and *shear crack models* for grain boundary sliding (GBS), it is now possible to compute the displacements across grain boundaries in a quantitative way and the results are in acceptable agreement with experiments. This has given a dramatic improvement in the understanding of GBS. The previous observations that the amount of grain boundary sliding is proportional to the creep strain are reproduced by the model. According to the shear sliding model the displacement is proportional to the grain size: This has been verified experimentally for small grain sizes, but the grain size dependence is probably exaggerated for larger grain sizes. A detailed comparison between the shear crack model and experiments is more difficult, since in none of the published results on GBS, full details of the particle structure are presented.

It is assumed in general that nucleation of creep cavities is based on GBS. The new models for GBS have made it possible to set up realistic models for nucleation. Many models for nucleation developed in the past are strongly stress dependent and suggest that the amount of cavitation would increase with stress, which is clearly at variance with most observations on creep. This applies for example to models based on classical nucleation theory. Using Lim's model for substructure induced cavitation [40], it has now been demonstrated both

for commercial copper and austenitic stainless steel that the creep stresses in the substructure are sufficiently high to nucleate cavities. Since the stresses are stationary, the problem with rapid relaxation in particular at high stresses is avoided. If particles instead of subgrain corners constrain the grain boundary dislocations, the outcome of the model is essentially the same. The model is consequently applicable to cavity nucleation at particles as well.

With the help of the *double ledge model* it can be explained why the nucleation rate is proportional to the creep strain rate. According to the model nucleation takes place when subgrain boundaries meet subgrain corners on the other side of a sliding grain boundary. The displacement rate is proportional to creep strain rate according to the GBS models. As a consequence the suboundaries will meet the subgrain corners at the same rate and this explains why the nucleation rate is proportional to the strain rate.

Harris developed a model for nucleation around particles many years ago [47, 48]. He considered the relation between particle sizes and the GBS displacement. If the particles are sufficiently large it is assumed that they will prevent GBS. He formulated a criterion for the critical particle size. If GBS is prevented significant stresses are formed at the particles. If the critical particle size is exceeded, Harris proposed that cavity nucleation can take place. With the event of the new models for GBS it has now for the first been possible to test Harris' ideas. It turns out that both the critical particle radius and the number of cavities that can be estimated from the particle distributions are in agreement with observations for austenitic stainless steels. In this way a method for estimating the critical particle size for nucleation has been established.

GBS does not occur on every grain boundary. In fact only on a limited number of GBS events is observed in a material that has been creep exposed [19]. As a consequence cavity nucleation only occurs on some grain boundaries. The presence of cavities show a large statistical variation, see for example [39]. The models in the present paper represent grain boundaries where cavities will be formed. These are also the grain boundaries that control the rupture of the material. The models predict a fairly high nucleation rate that represents the most active grain boundaries and not an average over all grain boundaries.

Models for cavity growth have been available for a long time. Unfortunately these models in general generate growth rates that are much higher than the observed ones. This might be the reason why very few quantitative comparisons have been made between experiments and models in the literature. A major step forward was the introduction of constrained growth [17]. Then the cavities were not allowed to grow faster than the surrounding creeping material. A quantitative model for constrained growth was given by Rice [18]. Still the growth rates tended to be higher than the observed ones. Only recently it has been recognised that some minor approximations in the work of Rice were essential to correct [52]. With these new corrections satisfactory predictions for cavity growths in austenitic stainless have been achieved.

The recent development has implied that quantitative models are now available for grain boundary sliding, for the thermodynamic feasibility of cavity nucleation controlled by subboundaries, the nucleation rate and constrained cavity growth, that is, for all of the involved

main processes. Each model is of great significance in itself, but by using combinations of them, the development of cavities can be fully understood.

7. Conclusions

1. Recent development of processes concerning the development of creep cavities has been reviewed. Models have been covered for grain boundary sliding, cavity nucleation and cavity growth.
2. Based on analysis of previously presented FEM models, a model for the grain boundary displacement during sliding called the shear sliding model has been presented. The model gives a displacement that is proportional to the creep strain. The model can quantitatively reproduce the observed displacements for fcc alloys.
3. Using Lim's model for subboundary assisted cavity nucleation, it has been demonstrated that this process is thermodynamically feasible for copper and for austenitic stainless steels. It gives a minimum cavitation stress that is well below stresses in creep exposed components.
4. According to the double ledge model, nucleation is assumed to take place when subboundaries on one side of a sliding grain boundary meet subgrain corners or particles on the other side. The model gives a nucleation rate that is proportional to the creep rate in good accordance with observations. The model can predict the measured nucleation rates in austenitic stainless steels.
5. Due to the development of the new models for GBS, it has for the first time been possible to test Harris' model for cavity nucleation around particles. The model gives a relation between the critical particle radius and the GBS velocity. Data for austenitic stainless steels confirm the validity of the model.
6. A modified constrained growth model has been presented. It gives lower growth rates than previous models. These lower growth rates have implied that observed growth rates for austenitic stainless steels can now be reproduced.
7. Alloys can fail by ductile or brittle creep rupture. It is demonstrated that by considering both ductile and brittle rupture, the prediction of creep rupture curves can be improved in particular at high temperatures and low stresses.

Author details

Rolf Sandström* and Junjing He

*Address all correspondence to: rsand@kth.se

Materials Science and Engineering, KTH Royal Institute of Technology, Stockholm, Sweden

References

[1] B. Neubauer, Recent Advances in Creep and Fracture of Engineering Materials and Structures, B. Wilshire, D.R.J. Owen (eds.). Pineridge Press, Swansea, 1981, 617–619.

[2] B. Neubauer, F. Arens-Fischer, Determination of residual life of power station components subject to creep stress, VGB Kraftwerkstechnik, 63 (1983) 637–645.

[3] L.M. Kachanow, Izvestiya Akademii Nauk SSSR, Otdelenie Tekhnicheskikh Nauk, Mekhanika i Mashinostroenie, 8 (1958), 26–31.

[4] Kachanow, L.M., Foundations of Fracture Mechanics. Moscow, 1974.

[5] Rabotnov, Y.N., Creep Problems in Structural Members. NorthHolland, Amsterdam, 1969.

[6] R. Sandstrom, A. Kondyr, Model for Tertiary-Creep in Mo and CrMo-Steels, in: Proceedings—Computer Networking Symposium, 1980, 275–284.

[7] R. Sandstrom, A. Kondyr, Creep Deformation, Accumulation of Creep Rupture Damage and Forecasting of Residual Life for Three Mo- and CrMo-Steels, VGB Kraftwerkstechnik, 62 (1982), 802–813.

[8] R. Sandstrom, Basic Model for Primary and Secondary Creep in Copper, Acta Materialia, 60 (2012) 314–322.

[9] M.H. Yoo, H. Trinkaus, Crack and Cavity Nucleation at Interfaces During Creep, Metallurgical Transactions A, 14 (1983) 547–561, doi:10.1007/BF02643772

[10] R. Raj, M.F. Ashby, Intergranular Fracture at Elevated Temperature, Acta Metallurgica, 23 (1975) 653–666.

[11] E. Smith, J.T. Barnby, Crack Nucleation in Crystalline Solids, Metal Science, 1 (1967) 56–64.

[12] R. Raj, Nucleation of Cavities at Second Phase Particles in Grain Boundaries, Acta Metallurgica, 26 (1978) 995–1006.

[13] H. Riedel, Life Prediction Methods for Constrained Grain Boundary Cavitation, International Journal of Pressure Vessels and Piping, 39 (1989) 119–134.

[14] X.G. Jiang, J.C. Earthman, F.A. Mohamed, Cavitation and Cavity-Induced Fracture During Superplastic Deformation, Journal of Materials Science, 29 (1994) 5499–5514.

[15] D. Hull, D.E. Rimmer, The Growth of Grain Boundary Voids Under Stress, Philosophical Magazine, 4 (1959) 673–687.

[16] W. Beere, M.V. Speight, Creep Cavitation by Vacancy Diffusion in Plastically Deforming Solid, Metal Science, 21 (1978) 172–176.

[17] B.F. Dyson, Constraints on Diffusional Cavity Growth Rates, Metal Science, 17 (1976) 349–353.

[18] J.R. Rice, Constraints on the Diffusive Cavitation of Isolated Grain Boundary Facets in Creeping Polycrystals, Acta Metallurgica, 29 (1981) 675–681.

[19] R. Sandström, R. Wu, J. Hagström, Grain Boundary Sliding in Copper and its Relation to Cavity Formation During Creep, Materials Science and Engineering A, 651 (2016) 259–268.

[20] C.W. Chen, E.S. Machlin, Trans. AIME J. Metals, 209 (1957) 829–835.

[21] J. Intrater, E.S. Machlin, J. Inst. Metals, 88 (1959/60) 305–310.

[22] B.J. Cane, Mechanistic Control Regimes for Intergranular Cavity Growth in 2. 25Cr-1Mo Steel Under Various Stresses and Stress States, Metal Science, 15 (1981) 302–310.

[23] D.J. Gooch, Creep Fracture of 12Cr-Mo-V Steel, Metal Science, 16 (1982) 79–89.

[24] J. He, R. Sandström, Modelling Grain Boundary Sliding During Creep of Austenitic Stainless Steels, Journal of Materials Science, 51 (2016) 2926–2934.

[25] D. McLean, M.H. Farmer, The Relation During Creep Between Grain-Boundary Sliding, Sub-Crystal Size and Extension, Journal of the Institute of Metals, 85 (1957) 41–50.

[26] N.G. Needham, J.E. Wheatley, G.W. Greenwood, The Creep Fracture of Copper and Magnesium, Acta Metallurgica, 23 (1975) 23–27.

[27] N.G. Needham, T. Gladman, Nucleation and Growth of Creep Cavities in a Type 347 Steel, Metal Science, 14 (1980) 64–72.

[28] R. Wu, R. Sandstrom, Strain Dependence of Creep Cavity Nucleation in Low Alloy and 12%Cr Steels, Journal of Materials Science & Technology, 12 (1996) 405–415.

[29] K. Pettersson, A Study of Grain Boundary Sliding in Copper With and Without an Addition of Phosphorus, Journal of Nuclear Materials, 405 (2010) 131–137.

[30] A. Ayensu, T.G. Langdon, The Inter-Relationship Between Grain Boundary Sliding and Cavitation During Creep of Polycrystalline Copper, Metallurgical and Materials Transactions A: Physical Metallurgy and Materials Science, 27 (1996) 901–907.

[31] F.W. Crossman, M.F. Ashby, The Non-Uniform Flow of Polycrystals by Grain-Boundary Sliding Accommodated by Power-Law Creep, Acta Metallurgica, 23 (1975) 425–440.

[32] F. Ghahremani, Effect of Grain Boundary Sliding on Steady Creep of Polycrystals, International Journal of Solids and Structures, 16 (1980) 847–862.

[33] H. Riedel, Cavity Nucleation at Particles on Sliding Grain Boundaries. A Shear Crack Model for Grain Boundary Sliding in Creeping Polycrystals, Acta Metallurgica, 32 (1984) 313–321.

[34] Laha K, Kyono J, Sasaki T, Kishimoto S, Shinya N Improved Creep Strength and Creep Ductility of Type 347 Austenitic Stainless Steel Through the Self-Healing Effect of Boron for Creep Cavitation, Metallurgical and Materials Transactions A, 36A (2005) 399–409.

[35] Kishimoto S, Shinya N, Tanaka H, Grain Boundary Sliding and Surface Cracking during Creep of 321 Stainless Steel, Materials, 37 (414) (1987) 289–294.

[36] Gates RS, Stevens RN, The Measurement of Grain Boundary Sliding in Polycrystals, Metallurgical Transactions, 5 (1974) 505–510.

[37] Gittins A, The Kinetics of Cavity Growth in 20 Cr25 Ni Stainless Steel, Journal of Materials Science, 5 (1970) 223–232.

[38] Morris DG, Harries DR, Wedge Crack Nucleation in Type 316 Stainless Steel, Journal of Materials Science, 12 (1977) 1587–1597.

[39] T.G. Langdon, The Role of Grain Boundaries in High Temperature Deformation, Materials Science and Engineering A, 166 (1993) 67–79.

[40] L.C. Lim, Cavity Nucleation at High Temperatures Involving Pile-ups of Grain Boundary Dislocations, Acta Metallurgica, 35 (1987) 1663–1673.

[41] P.J. Henderson, R. Sandstrom, Low Temperature Creep Ductility of OFHC Copper, Materials Science and Engineering A, 246 (1998) 143–150.

[42] ECCC European Creep Collaborative Committee Data Sheets 2005—HR3C.120, 2005.

[43] R. Sandström, R. Wu, Influence of Phosphorus on the Creep Ductility of Copper, Journal of Nuclear Materials, 441 (2013) 364–371.

[44] J. He, R. Sandström, Formation of Creep Cavities in Austenitic Stainless Steels, Journal of Materials Science, 51 (2016) 6674–6685.

[45] Hong JH, Nam SW, Choi SP, The Influences of Sulphur and Phosphorus Additions on the Creep Cavitation Characteristics in Type 304 Stainless Steels, Journal of Materials Science 21 (11) 3966–3976.

[46] Laha K, Kyono J, Shinya N, Suppression of Creep Cavitation in Precipitation-Hardened Austenitic Stainless Steel to Enhance Creep Rupture Strength. Transactions of the Indian Institute of Metals, 63 (2–3) (2010) 437–441.

[47] J.E. Harris, An Analysis of Creep Ductility of Magnox Al80 and its Implications, Journal of Nuclear Materials, 15 (1965) 201–207.

[48] J.E. Harris, Nucleation of Creep Cavities in Magnesium, Transactions of the Metallurgical Society of AIME, 233 (1965) 1509.

[49] O.R. Arzate, L. Martinez, Creep Cavitation in Type 321 Stainless Steel, Material Science and Engineering A, 101 (1988) 1–6.

[50] K. Laha, J. Kyono, T. Sasaki, S. Kishimoto, N. Shinya, Improved Creep Strength and Creep Ductility of Type 347 Austenitic Stainless Steel through the Self-Healing Effect of Boron for Creep Cavitation, Metallurgical and Materials Transactions A, 36A (2005) 399-409.

[51] K. Davanas, A.A. Solomon, Theory of Intergranular Creep Cavity Nucleation, Growth and Interaction, Acta Metallurgica et Materialia, 38 (1990) 1905–1916.

[52] J. He, R. Sandström, Creep Cavity Growth Models for Austenitic Stainless Steels, Materials Science and Engineering A, 674 (2016) 328–334.

[53] S. Vujic, R. Sandstrom, C. Sommitsch, Precipitation Evolution and Creep Strength Modelling of 25Cr20NiNbN Austenitic Steel, Materials at High Temperatures, 32 (2015) 607–618.

[54] J. He, R. Sandström, Basic Modelling of Creep Rupture in Austenitic Stainless Steels, to be publ. (2017).

[55] NRIM, National Research Institute for Metals, Tokyo, Japan, 1987.